

STP 1620, 2020 / available online at [www.astm.org](http://www.astm.org) / doi: 10.1520/STP162020180111

Richard A. Livings,<sup>1</sup> Eric J. Biedermann,<sup>1</sup> Chen Wang,<sup>2</sup>  
Thomas Chung,<sup>2</sup> Steven James,<sup>3</sup> Jess M. Waller,<sup>4</sup>  
Scott Volk,<sup>5</sup> Ajay Krishnan,<sup>5</sup> and Shane Collins<sup>6</sup>

# Nondestructive Evaluation of Additive Manufactured Parts Using Process Compensated Resonance Testing

## Citation



R. A. Livings, E. J. Biedermann, C. Wang, T. Chung, S. James, J. M. Waller, S. Volk, A. Krishnan, and S. Collins, "Nondestructive Evaluation of Additive Manufactured Parts Using Process Compensated Resonance Testing," in *Structural Integrity of Additive Manufactured Parts*, ed. N. Shamsaei, S. Daniewicz, N. Hrabe, S. Beretta, J. Waller, and M. Seifi (West Conshohocken, PA: ASTM International, 2020), 165–205. <http://doi.org/10.1520/STP162020180111><sup>7</sup>

## ABSTRACT

Variations in build process parameters, post-processing parameters, and feedstock have a significant impact on the structural integrity and performance of components made with additive manufacturing (AM). Effective nondestructive testing (NDT) is critical for ensuring the structural integrity of components. Complex geometries, nonequilibrium microstructures, new process variables, and lack of clear accept or reject criteria for AM components present new challenges to NDT. Quantitative, volumetric NDT methods that can detect material defects of interest in complex geometries are required. Process


---

Manuscript received November 2, 2018; accepted for publication February 7, 2019.

<sup>1</sup>Vibrant Corp., 8916 Adams St. NE, Albuquerque, NM 87113, USA R. A. L.  <http://orcid.org/0000-0002-8864-4761>, E. J. B.  <http://orcid.org/0000-0001-7551-1997>

<sup>2</sup>Northrop Grumman Aerospace Systems, 700 North Douglas, El Segundo, CA 90245, USA

<sup>3</sup>Aerojet-Rocketdyne, 134 Dickenson Ave., Newbury Park, CA 91320, USA

<sup>4</sup>NASA-JSC White Sands Test Facility, Laboratories Dept., MS 200LD, Las Cruces, NM 88004, USA  <http://orcid.org/0000-0002-7847-8376>

<sup>5</sup>Incodema3D, 330 Main St., Suite A, Freeville, NY 13068, USA A. K.  <http://orcid.org/0000-0001-5237-8038>

<sup>6</sup>Additive Industries North America, Inc., 1250 Avenida Acaso, Unit H, Camarillo, CA 93012, USA

<sup>7</sup>ASTM Symposium on *Structural Integrity of Additive Manufactured Parts* on November 6–8, 2018 in Washington, DC, USA.

compensated resonance testing (PCRT) is an NDT method that uses a swept sine input to excite the component's resonance modes of vibration. The resonance frequencies are recorded, analyzed statistically, and compared to acceptability limits established using a database of training components. The swept sine input excites whole-body vibrational modes in nearly any geometry, and the component's resonance frequencies correlate directly to its structural integrity. In this study, PCRT evaluations were performed on titanium alloy (Ti-6Al-4V) populations made with electron beam PBF and aluminum alloy (AlSi10Mg) populations made with laser PBF. The evaluations were conducted in support of ASTM round-robin testing. In the Ti-6Al-4V population, PCRT showed clear resonance frequency differences between nominal specimens and off-nominal specimens with defective material states. PCRT also quantified the effects of hot isostatic pressing (HIP). PCRT pass/fail NDT of the Ti-6Al-4V population in the pre-HIP and post-HIP states demonstrated 100% accuracy. Computed tomography scans of the post-HIP specimens showed no clear indications of porosity. Follow-up tensile testing of a subset of nominal and off-nominal specimens in the post-HIP state showed that the off-nominal specimens had lower yield stresses and ultimate tensile stresses than nominal specimens. In the AlSi10Mg population, PCRT detected differences between recycled and virgin feedstock powder. PCRT pass/fail NDT of AlSi10Mg specimens exposed to nominal and off-nominal heat treatment demonstrated 100% accuracy.

### Keywords

process compensated resonance testing (PCRT), additive manufacturing, nondestructive testing, nondestructive evaluation, nondestructive inspection, NDT, NDE, NDI

## Introduction

The rapid growth of additive manufacturing (AM) technology and applications has outpaced the development of standards and best practices for performing nondestructive testing (NDT) on additively manufactured components. Many commercial, academic, and government entities are producing AM components, while the NDT and engineering communities are still establishing testing and qualification criteria. The lack of accepted qualification and certification procedures have hindered the use of AM components in aerospace. To address this gap, an ASTM workgroup was formed by the E07.10 subcommittee to develop ASTM [E3166](#), *Standard Guide for Nondestructive Examination of Metal Additively Manufactured Aerospace Parts after Build*.<sup>1</sup> The guide discusses the use of a variety of NDT procedures for NDT for AM parts. A companion project undertaken by the workgroup was round-robin NDT of AM physical reference standards and test articles obtained from a variety of sources.<sup>2</sup> The goal of the round-robin testing was to demonstrate NDT capabilities for AM components, use that knowledge to drive development of the standard guide, and identify effective NDT tools for different defects and material states.

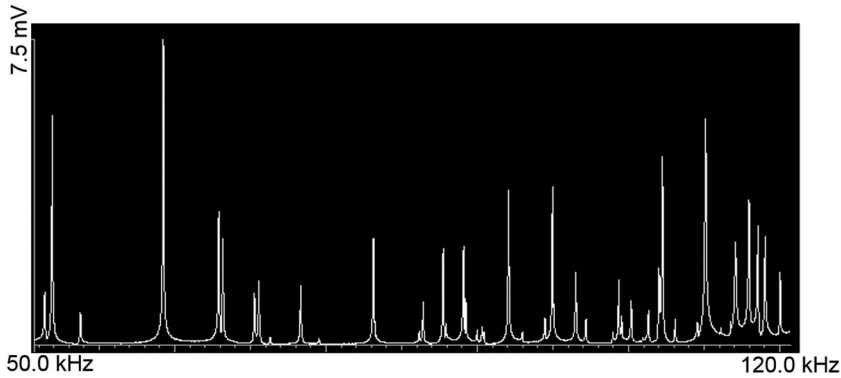
The reproducibility of PBF parts depends on factors such as feedstock, equipment, process, defects, microstructural variation, surface roughness, residual stress, and post-processing. These factors determine finished part properties, and ultimately, whether a part is acceptable for use. Against this backdrop of property variation, mitigation against part failure relies mainly on NDT to detect defects or off-nominal behavior, and destructive (e.g., proof) tests to assess the effect of defects on part performance. Additional challenges for NDT for AM components include part complexity, access to the inspection surface or inspection volume, flaw orientation (especially detectability of planar flaws), surface roughness interferences, and the lack of clear accept and reject criteria based on allowable defect type, size, and distribution.<sup>3–6</sup> Complex “design-to-constraint” parts categorized as having high “AM risk”<sup>6</sup> will often have regions inaccessible to many NDT techniques, including computed tomography (CT), eddy current testing (ET), radiologic testing (RT), and ultrasonic testing (UT), precluding reliable inspection. In these cases, PCRT may be one of the few available NDT techniques for part qualification. PCRT is a volumetric resonance inspection that excites and analyzes the resonance modes of vibration for the entire part. The resonance frequencies of a component correlate directly to the component material state, making PCRT an effective NDT tool for detecting components that are at risk for structural failure in service.

In this study, Vibrant Corporation applied PCRT to several sample populations having different build process histories (nominal versus off-nominal builds), post-processing (hot isostatic pressing [HIP] and nominal versus off-nominal heat treatments), and feedstock material (virgin versus recycled powder). Because PCRT provides accurate, fast, and quantitative resonance frequency information that correlates directly to a part’s material state, the goal of this study was to demonstrate PCRT detection of material state differences and to show that changes in the PCRT response correlated with changes in mechanical performance and, therefore, structural integrity. Linking PCRT response with part performance was accomplished by subjecting a subset of ASTM E8, *Standard Test Methods for Tension Testing Methods of Metallic Materials*–compliant dog-bone specimens to mechanical testing<sup>7</sup> and correlating the PCRT data to the tensile test results. CT and fractography also were used on the same specimens to further characterize the material state and understand the correlations between the material state differences detected by PCRT and the performance differences revealed by tensile testing.

## Materials and Methods

### PCRT FUNDAMENTALS

PCRT is based on a fundamental physical property of solid objects: any rigid component will resonate at specific frequencies that are a function of its mass, shape, and material properties. Material alterations or flaws, process deviations, raw material inputs and accumulation of in-service damage can change the normal resonant

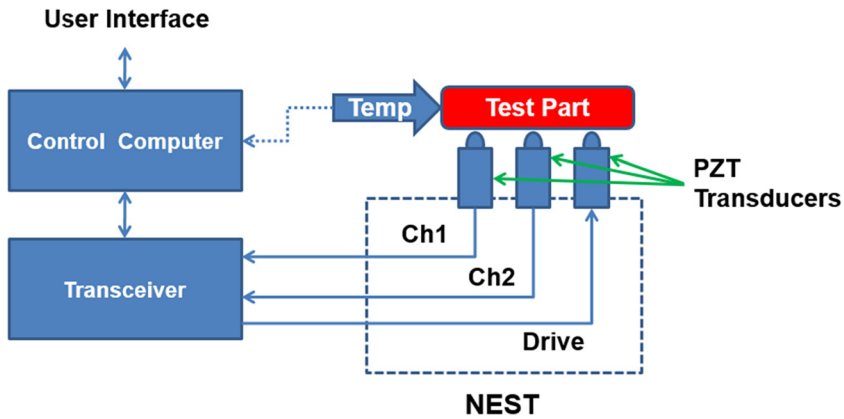
**FIG. 1** PCRT broadband resonance spectrum.

pattern of components. PCRT uses resonant ultrasound spectroscopy (RUS) to collect the resonance frequencies of a component using a swept sine input that excites all the resonance modes within a broadband frequency range configured for that material-geometry combination. The use of RUS to collect resonance frequency spectra for parts is described in ASTM E2001, *Standard Guide for Resonant Ultrasound Spectroscopy for Defect Detection in Both Metallic and Non-Metallic Parts*.<sup>8</sup> An example of broadband resonance spectrum is shown in figure 1. PCRT combines the RUS frequency data with pattern recognition and statistical analysis algorithms that detect material state variations in components while compensating for normal manufacturing variations that may obscure out-of-specification conditions with conventional RUS.

### Resonance Spectrum Data Collection

The PCRT system includes the control computer, the transceiver, and the test fixture (fig. 2). The control computer is a standard PC with the PCRT software installed. PCRT software controls resonance frequency data collection and performs statistical analysis on the frequency data. The software outputs automated pass/fail testing results requiring no operator interpretation. The transceiver is a high-end signal generator and spectrum analyzer. The test fixture, or nest, includes a set of lead zirconate titanate ( $\text{PbZr}_x\text{Ti}_{(1-x)}\text{O}_3$  or PZT) transducers that contact the part. One transducer excites the part with a swept sine waveform, and the other two transducers receive the resonance response.

Data collection and analysis for all sample populations began with configuration of a PCRT fixture and data collection settings. The fixture includes the transducer arrangement used to hold the part during testing, plus any tooling used to guide part placement. The transducer arrangement chosen for any part is an optimization between data quality, and rapid, repeatable part placement. Changing how

**FIG. 2** PCRT system schematic.

the transducers contact the part typically has an insignificant effect on the frequency of the resonance response, but it can produce some variation in the amplitude of the resonance response. PCRT uses resonance frequency for its analysis, not amplitude, so the transducer arrangement needs only to provide a strong enough signal for the resonance modes to be reliably identified by the PCRT peak-picking algorithm.

The specimens analyzed in this study were all axisymmetric specimens, which are typically held in a V-block test fixture like the laboratory-grade example shown in [figure 3](#). The V-block configuration uses three active transducers and adds a fourth, inactive, transducer to provide stable support for the part. [Figure 4](#) shows a production-grade PCRT test system with a V-block fixture utilizing hard-point tooling for rapid, repeatable part placement.

Data collection settings are composed of the range of frequencies scanned to record a broadband resonance spectrum, and the timing settings that govern the resolution and speed of the swept sine input. PCRT data collection settings are configured to be specific to a given part geometry and material. The timing settings are an optimization between data quality and data collection speed. The data collection settings for each sample population are described in the “Results and Discussion” section.

PCRT frequency measurements show high repeatability. Laboratory-grade fixtures like the ones used in this study produce frequency variation on the order of  $\pm 0.02\%$  or less for most resonance modes. Most of that variability comes from variation in part placement from scan to scan. Production-grade fixtures that use hard-point tooling with automated lifting of the transducers or robotic part placement have variation that is lower than laboratory-grade fixtures by an order of magnitude or better.

**FIG. 3** Laboratory grade V-block test fixture holding a Ti-6Al-4V cylindrical test specimen.

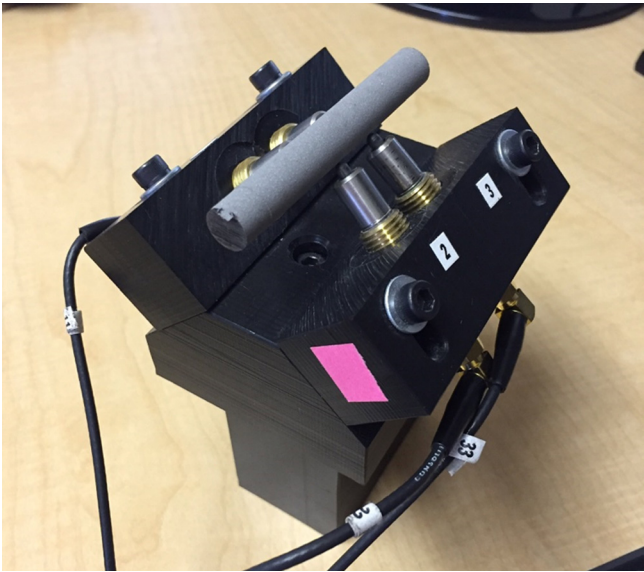
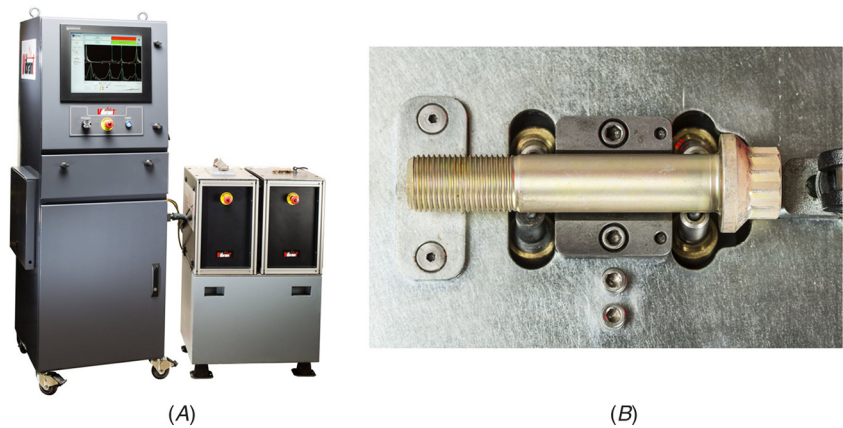


**FIG. 4** (A) Production-grade PCRT system; and (B) bolt specimen on production-grade V-block test fixture.



**PCRT ANALYSIS METHODS**

PCRT analysis can take several forms depending on the application. Applications may make use of targeted defect detection, population characterization, or part-to-

itself (PTI) comparisons. These analyses use pattern recognition or statistical tools to develop PCRT sorting modules that evaluate the frequency responses of tested components. In operational NDT in manufacturing or sustainment environments, PCRT sorting modules provide rapid, accurate, and operator-independent pass/fail assessments. In operational manufacturing applications, PCRT inspections can increase production yield, optimize part life, and significantly reduce field failures of components.

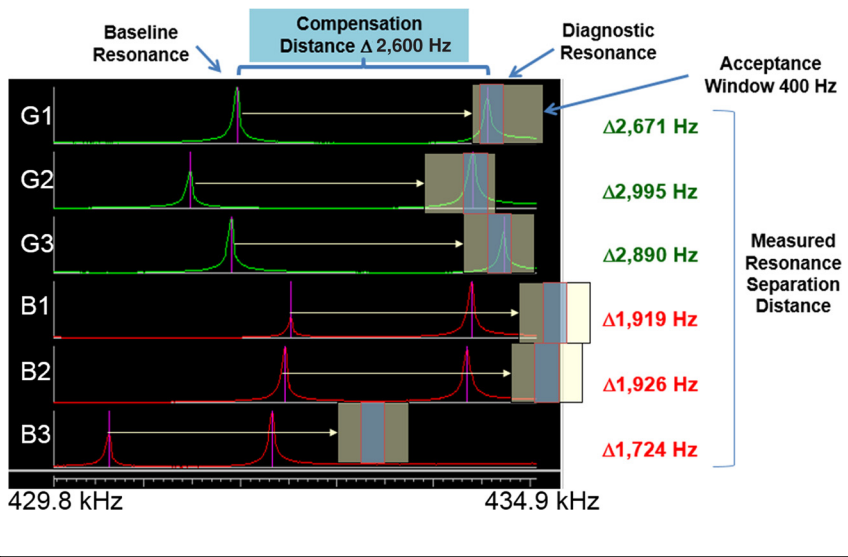
### PCRT Targeted Defect Detection

PCRT targeted defect detection sorting modules are configured to detect targeted material states, defects, processing variations, or geometric deviations. In these applications, a PCRT sorting module is trained with statistically significant populations of acceptable and unacceptable (parts with the conditions of interest) components. The resonance frequencies for a component under inspection are statistically scored for their similarity to the central tendencies of the acceptable and unacceptable training populations. The component passes if it is sufficiently similar to the known acceptable population and sufficiently different from the known unacceptable population. If the component is too different from the acceptable population or too similar to the unacceptable population it fails. ASTM Standard Practice E2534, *Standard Practice for Process Compensated Resonance Testing Via Swept Sine Input for Metallic and Non-Metallic Parts*,<sup>9</sup> describes the process for configuring PCRT targeted defect detection inspections and performing operation inspection with them.

To build a targeted defect detection inspection, broadband resonance spectra for the training components are collected and classified (acceptable, unacceptable, or other) according to the best available knowledge from the sample owner or follow-up inspection. The database of logged, classified resonance spectra is known as the training set. PCRT vibrational pattern recognition (VIPR) algorithms identify frequency patterns in the training set that differentiate the acceptable and unacceptable components. Diagnostic frequency patterns can include virtually any combination of resonance modes in the spectra. Figure 5 shows an example of a simple modal relationship defined by the frequency delta between two modes. The baseline and diagnostic resonance modes for acceptable components (G1, G2, and G3) have a frequency delta greater than 2,600 Hz. The frequency delta for unacceptable components (B1, B2 and B3) is less than 2,000 Hz.

The Mahalanobis-Taguchi system (MTS) is used to score the diagnostic frequency pattern data and optimize the number of modes used in the sorting module. The Mahalanobis component involves the calculation of the Mahalanobis Distance, essentially the similarity of a given part to the central tendency of the known acceptable and unacceptable populations. The similarity of a part to the known acceptable population for that part is called the MTS score. The similarity of a part to the known unacceptable population for that part is called the bias discriminator. The Taguchi component of the MTS optimizes the number of modes used for the

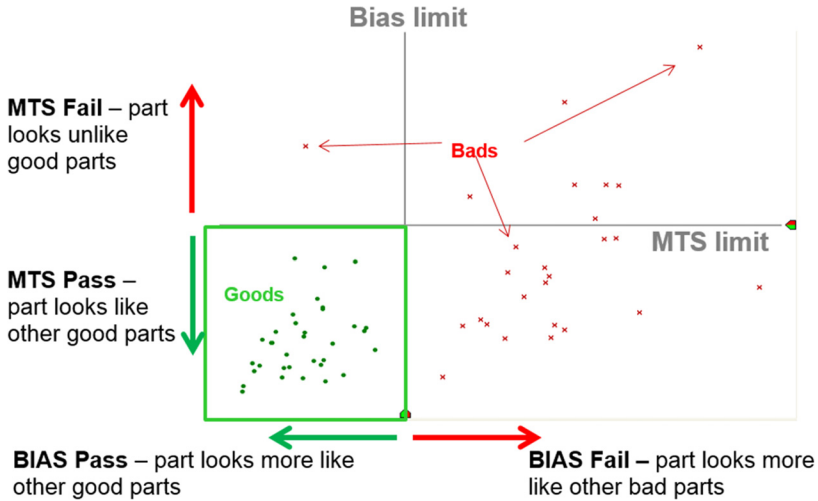
**FIG. 5** Resonance patterns: modes for acceptable parts (G1, G2, G3) separated by more than 2,600 Hz; modes for unacceptable parts (B1, B2, B3) separated by less than 2,000 Hz.<sup>8</sup>



calculation, focusing on the most diagnostic frequency patterns rather than using the full broadband spectra.<sup>9</sup>

Figure 6 shows an example of a VIPR plot for PCRT sorting module. The MTS limit (x-axis) is the pass/fail threshold for similarity to the acceptable components (dots). The bias limit (y-axis) is the pass/fail threshold for similarity to the unacceptable components (x's). Parts that fall within the MTS and bias limits pass the PCRT (lower left quadrant), and parts that exceed either limit (or both) fail. The PCRT system calculates MTS and bias scores automatically and returns a pass/fail result that requires no operator interpretation. During a production test, the operator sees a red light or green light indication depending on the test result. The MTS and bias scores, along with the raw frequency data, are all stored digitally in a reviewable test results file. Serialized parts, like turbine blades or landing gear wheels, have their serial numbers recorded along with the test results for traceability and use in PCRT PTI applications.

The PCRT software predicts the uncertainty in the pass/fail result for every component in the training population. This uncertainty is a function of the small level of frequency variation from scan to scan (see the section “Resonance Spectrum Data Collection” for more information on measurement repeatability) and the placement of the MTS and bias limits. The MTS and bias limits can be adjusted if the customer requires certain confidence limits for all of the acceptable and unacceptable populations, or if other business metrics, such as fallout rate in acceptable

**FIG. 6** VIPR plot for PCRT-targeted defect detection.

parts, must be considered. For the sample populations studied in this paper, the minimum confidence interval predicted for the most borderline training components was greater than 95.5%, corresponding to a coverage factor of  $k = 2$  or higher. Nearly all components in the population had confidence intervals greater than 99%, with a coverage factor of  $k = 2.5$  or higher.

### PCRT Population Characterization and Outlier Screening

PCRT population characterization and outlier screening are used in cases in which a population of known unacceptable components is not available, or classification data are uncertain or unavailable. These methods can be used to screen populations of parts for outlier material states when classification data for a targeted defect detection sort is not available. Both methods use a Z-score analysis of the broadband resonance frequency data. The Z-score analysis uses statistical scoring of the broadband resonance spectra (as opposed to scoring for a subset of diagnostic modes in targeted defect detection). Population characterization uses the Z-score to quantify variation within and between component lots in a population of parts. It can also identify individual outliers. A pass/fail sorting module can be configured to reject outliers automatically in an outlier screening approach. ASTM Standard Practice E3081, *Standard Practice for Outlier Screening Using Process Compensated Resonance Testing via Swept Sine Input for Metallic and Non-Metallic Parts*,<sup>10</sup> describes the application of PCRT for outlier screening. Outlier components can be characterized through additional inspection for possible defective material states and used to build up a known unacceptable training set for targeted defect detection.

The Z-score analysis begins with logging resonance frequency data for parts and building a database of resonance frequencies, as with targeted defect detection. A subset of the parts is designated as a reference set. In a production environment, the reference set can include parts that are presumed to be normal, acceptable production. They also can include qualification parts verified by the customer.

A typical Z-score analysis calculates two Z-score parameters: the average Z-score and Z-score standard deviation. The average Z-score quantifies bulk variation in resonance frequencies for a given part. A part with higher overall frequencies will have a higher Z-score average, and vice versa. The Z-score standard deviation quantifies variation in the frequency pattern for a given part. Parts that show greater peak-to-peak variation in frequencies have a higher Z-score standard deviation. When analyzing Z-score data, the Z-score standard deviation is plotted against the Z-score average in a scatter plot, with each point representing a different part. [Figure 7](#) shows an example of a Z-score plot. Each circular dot is an individual part from the normal population. Each diamond is an outlier part relative to the normal population.

In an outlier screening application, the Z-score for each component is compared with a bounding limit that specifies the maximum and minimum allowable Z-score average and Z-score standard deviation. The bounding limit is set to encompass the range of normal production. Limits can be elliptical or rectangular depending on the shape of the production reference set Z-score distribution. Parts

**FIG. 7** Example of a Z-score plot.

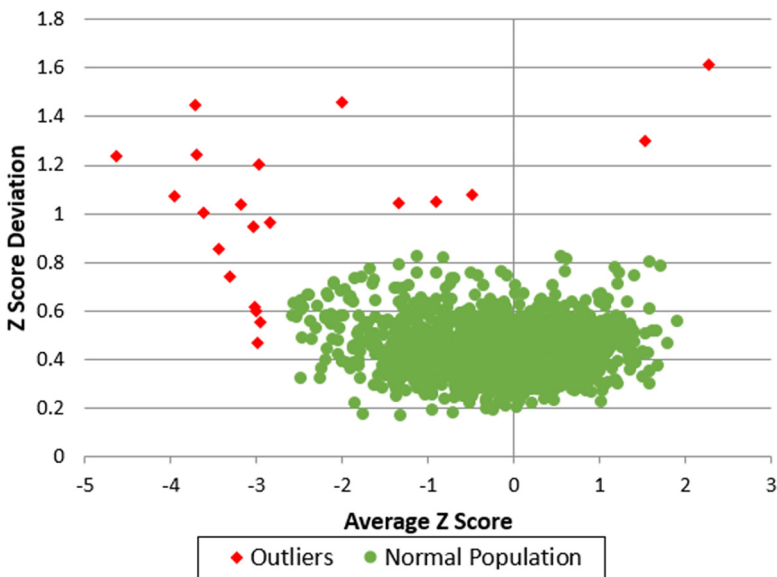
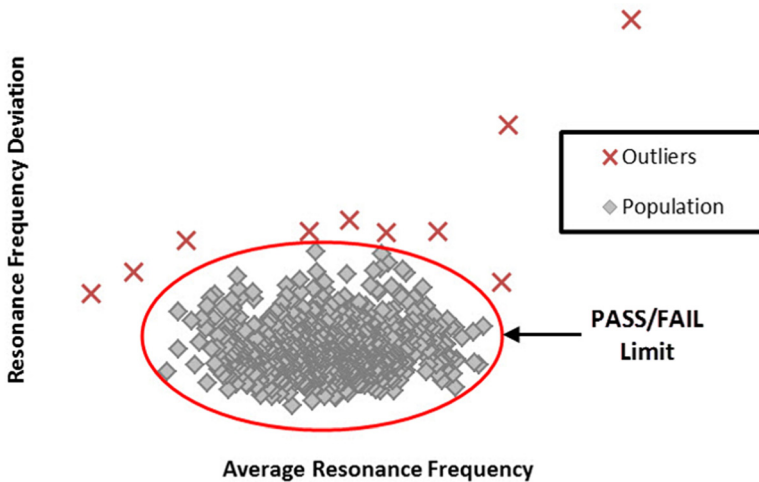


**FIG. 8** PCRT outlier screening illustration; rejected outliers exceed limits based on average frequency, frequency deviation or both.<sup>10</sup>



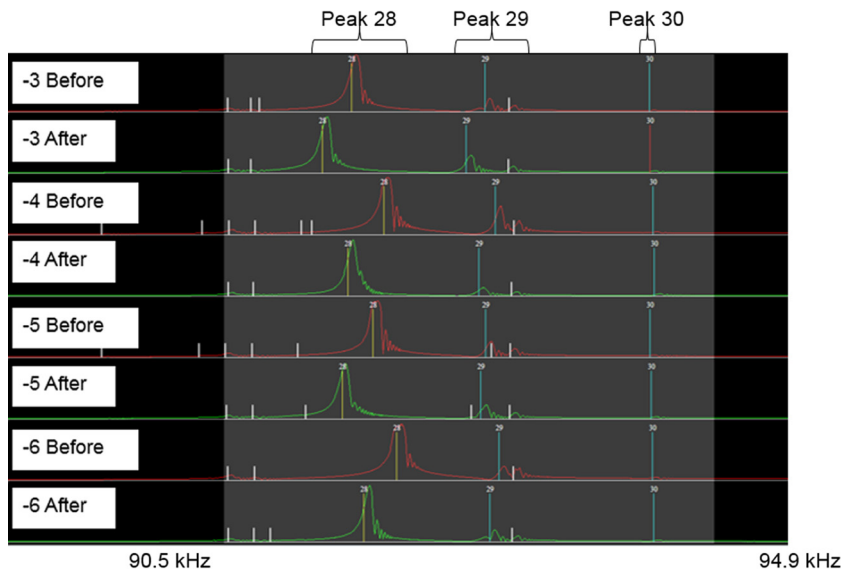
falling within the bounding box or ellipse pass, and parts with a Z-score average or Z-score standard deviation that exceeds the limits are rejected. The comparison of the test part Z-score to the bounding is automatic, generating a pass/fail result requiring no operator interpretation. Figure 8 illustrates PCRT outlier screening with an elliptical pass/fail limit. Outliers, indicated by an  $\times$ , have average frequency or frequency deviation values that exceed the pass/fail limit.

### PCRT PTI inspection

When performing a PCRT PTI inspection, frequency data are recorded for a serialized part before and after a manufacturing process step, a repair process step, or an interval of in-service use. The frequency change between the two frequency measurements is calculated and used to measure the effect of the process step or service interval on the part. Limits can be set on the frequency change to establish process monitoring/control and pass/fail inspection criteria. The PTI inspection can determine whether a processing step is within specification or whether accumulated damage remains within acceptable limits. ASTM Standard Practice E3213, *Standard Practice for Part-to-Itself Examination Using Process Compensated Resonance Testing via Swept Sine Input for Metallic and Non-Metallic Parts*,<sup>11</sup> describes the application of PCRT for PTI examination.

Figure 9 shows PTI data for steel components subjected to a hardening process. When components are hardened, sensitive modes show a measurable decrease in resonance frequencies. The case depth and hardness values for the induction-hardened region correlate to the magnitude of the frequency decrease. Process

FIG. 9 PCRT PTI data for the manufacturing process in steel components.<sup>11</sup>



control limits can be set for the PTI frequency change to ensure proper processing and alert users to process drift. Figure 10 shows a run chart for hardened steel components. Each dot represents an individual part. The y-axis is the frequency change between the PCRT measurements taken before and after hardening. The x-axis is a time index. The lines labeled “Upper Spec Limit” and “Lower Spec Limit” denote the minimum and maximum allowable frequency change, respectively.

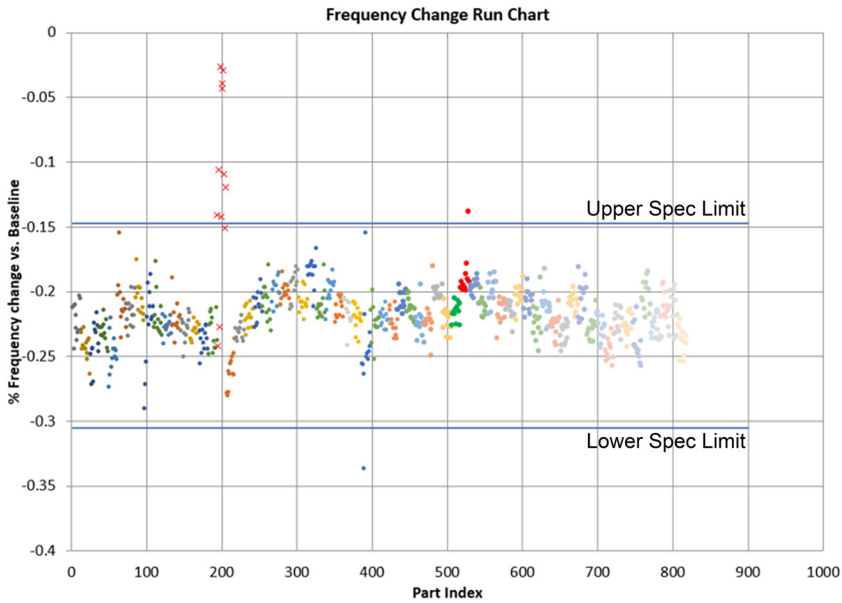
CT ANALYSIS METHODS

CT scanning at Northrop Grumman was performed with a GE Nanomex 180 system with a 180-kV/15-W X-ray source and 203.2-mm detector. The CT images were taken at 160-kV/80-μA/0.1-mm copper (Cu) filter, with 1,000 image frames each recorded at 1-s exposure. The GE Datos/x reconstruction software provided smoothing, beam hardening, and alignment correction for a tomograph with 48-μm pixel resolution. The area analyzed was a 50.8 mm column using VG Studio Max 2.2 (Volume Graphics).

MECHANICAL TESTING

Mechanical testing was used to verify material state differences in the PCRT data on a subset of nominal and off-nominal electron beam powder bed fusion (EB-PBF) Ti-6Al-4V dog-bone specimens. The mechanical tensile testing was performed per ASTM E8<sup>7</sup> at the Northrop Grumman Mechanical Test Lab. The tensile testing utilized a 90-kN (20,000-lb<sub>f</sub>) load cell (fig. 11). Tensile specimens were fitted

**FIG. 10** Run chart for hardening in steel components; dots represent individual parts and upper and lower spec limit lines represent minimum and maximum allowable frequency change, respectively



with a 2.5-cm (1-in.) extensometer with a data acquisition rate of 0.127 mm/mm/min (0.005 in./in./min). The tensile testing performed for this study was accomplished using a single machine and operator to maximize repeatability and reproducibility of results.

## SAMPLE POPULATIONS

### Ti-6Al-4V EB-PBF Dog-bone Specimens

Inspection for defective material states produced by AM build process variation using PCRT was demonstrated for a set of Ti-6Al-4V dog-bone specimens provided by MB CalRAM, LLC. The specimens were made with an EB-PBF process. Samples were tested with PCRT in the as-built state before HIP was performed and then tested again in the post-HIP state. The application of HIP allowed for a demonstration of a PCRT PTI comparison that looked for indications that HIP had a “healing” effect on the defective material state. CalRAM produced test specimens in two build cycles: one built with nominal process parameters and another with off-nominal process parameters.

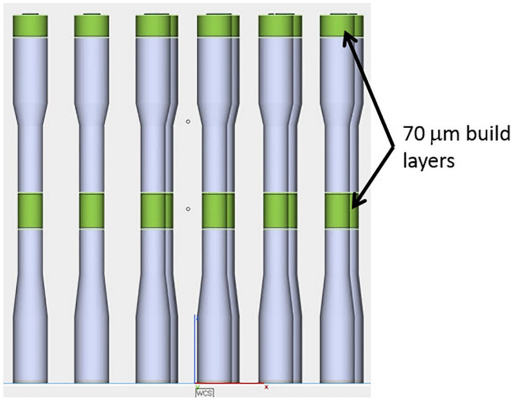
The EB-PBF process uses a dynamic energy density formula that is based on the melt cross-sectional area of each layer. The build programmer typically does

**FIG. 11** Tensile testing load cell at Northrop Grumman Mechanical Test Lab holding a CalRAM Ti-6Al-4V ASTM E8 dog-bone test specimen (approved for public release: NG 18-1423 dated July 2, 2018).



not have control over beam energy or scan speed. Therefore, CalRAM used layer thickness to intentionally create a defective material state in specific regions. This was accomplished by stitching in the Z direction different STL files that had been sliced at different thicknesses. CalRAM built the nominal population with a 50- $\mu\text{m}$  melt theme and 50- $\mu\text{m}$  layer thickness intended to produce a nominal material state. [Figure 12](#) shows a diagram of the off-nominal specimens, with sections in the gauge and grip regions built with a 50- $\mu\text{m}$  melt theme and 70- $\mu\text{m}$  actual layer thickness designed to produce a defective material state by inputting lower-than-necessary energy density. CalRAM's goal was not to make a specific defect, but to ensure a defective material state that would affect structural performance. The samples were described by CalRAM as having lack-of-fusion (LOF) porosity when they were sent to Vibrant. Because the exact state of the microstructure was not known at manufacture, the specimens are described as "off-nominal" in this paper.

**FIG. 12** Ti-6Al-4V off-nominal dog-bone schematic; indicated sections were 70- $\mu$ m layers, but printed with a 50- $\mu$ m energy density theme.



CalRAM supplied Vibrant with 28 nominal (Build MOR3050) and 28 off-nominal (Build MOR3014) samples in the pre-HIP state (fig. 13). After HIP, 20 specimens from each sample population were returned to Vibrant. A summary of the sample population is given in table 1.

**FIG. 13** CalRAM Ti-6Al-4V ASTM E8 dog-bone test specimens.



**TABLE 1** Description of CalRAM Ti-6Al-4V sample population

Lot Number	Quantity	Classification	State	Build Parameters
MOR3050	28	Nominal	As-built	50- $\mu$ m melt theme; 50- $\mu$ m layer thickness
MOR3014	28	Off-Nominal	As-built	50- $\mu$ m melt theme, 70- $\mu$ m layer thickness
MOR3050	20	Nominal	Post-HIP	50- $\mu$ m melt theme; 50- $\mu$ m layer thickness
MOR3014	20	Off-Nominal	Post-HIP	50- $\mu$ m melt theme, 70- $\mu$ m layer thickness

**AlSi10Mg LB-PBF Cylindrical Specimens**

The effect of post-build processing variation and feedstock powder material variation was investigated using PCRT for a set of AlSi10Mg cylindrical specimens made from a laser powder bed fusion (LB-PBF) process. Incodema3D provided three sample populations made from three different builds. Per the descriptions provided by Incodema3D, Serial A was made with optimal build parameters, optimal stress relief heat treatment, and virgin powder. Serial B was made with optimal build parameters, suboptimal stress relief heat treatment, and virgin powder. Serial B’s suboptimal stress-relief heat-treatment process introduced variation in the exposure time, temperature, and cooling procedure to alter the thermal history of the part. Serial C was made with optimal build and stress-relief heat-treatment parameters but was made from recycled powder. [Table 2](#) summarizes the Incodema3D sample population. [Figures 14](#) and [15](#) show the AlSi10Mg specimen populations on their respective build plates.

**Results and Discussion**

**PCRT ANALYSIS OF TI-6AL-4V EB-PBF DOG-BONE SPECIMENS**

**Analysis of As-Built Specimens**

Data collection for the Ti-6Al-4V specimens began with the configuration of the test fixture and data collection settings. [Figure 16](#) shows the V-block transducer arrangement. Resonance spectra were collected across a frequency range of 1.3 to 250.0 kHz. Data quality and measurement repeatability were considered good for this study based on low-noise spectra with high Q (quality factor) resonance peaks and measurement variations of less than  $\pm 0.02\%$  for repeated measurements.

Several PCRT analyses were utilized in this study. A PCRT population characterization was completed for both the as-built and post-HIP states using a statistical Z-score analysis. A VIPR targeted defect detection analysis was employed in both states to determine whether the microstructural defects were detectable using PCRT and whether the two groups were distinguishable after HIP. PTI examination was

**TABLE 2** Description of Incode<sup>®</sup>3D AlSi10Mg sample population

Group	Quantity	Powder	Build Parameters	Stress Relief Heat Treatment	Heat Treatment Temperature, °C	Heat Treatment Time, h	Cooling
Serial A	30	Virgin	Optimal (stock EOS for 30 µm LT AlSi10Mg)	Optimal	298.89	2.0	Air cool on rack
Serial B	30	Virgin	Optimal (stock EOS for 30 µm LT AlSi10Mg)	Suboptimal	307.22	2.5	Cool in oven, door ajar 45 min, then air cool on rack
Serial C	6	Recycled and Blended Single Lot	Optimal (stock EOS for 30 µm LT AlSi10Mg)	Optimal	298.89	2.0	Air cool on rack

**FIG. 14** Build plates for nominal (Serial A) and suboptimal heat-treatment (Serial B) sample populations.

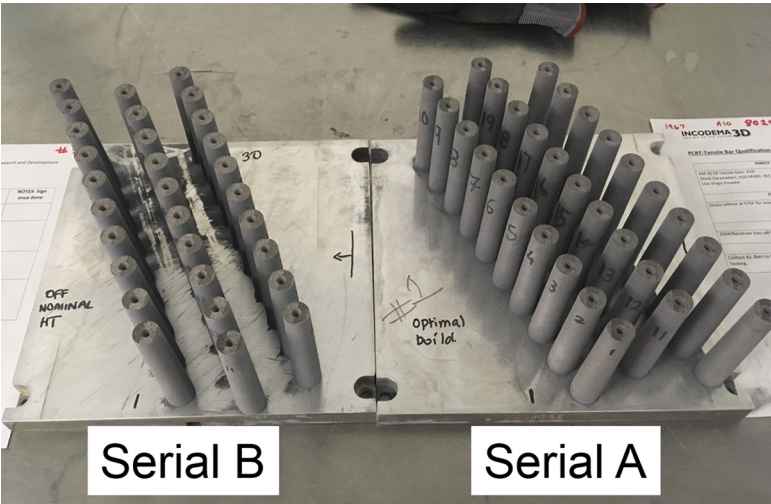
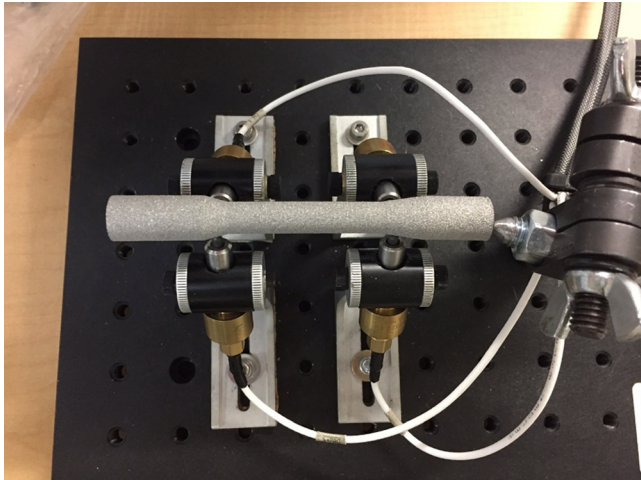


**FIG. 15** Build plates for recycled powder (Serial C) population.



**FIG. 16** PCRT fixture for CalRAM Ti-6Al-4V ASTM E8 dog-bones.



used to quantify the effects of HIP and to look for indications that HIP affected the nominal and off-nominal samples differently.

The results from the population characterization Z-score analysis of the dog-bone specimens in the as-built state are shown in [figure 17](#). Fifty-one resonance modes were used in this analysis. The nominal group was used as the reference group. Clear differences in resonance behavior between the two groups were observed, with a significant gap in the Z-score standard deviation. This indicated that the microstructural defects in the off-nominal population increased the variability of resonance behavior versus the nominal population. This was the expected result for a localized defective condition, which typically affects some modes of vibration more than others, producing the spectra pattern variation that would cause higher Z-score standard deviation values.

A targeted defect detection inspection using a VIPR analysis was trained to pass all nominal parts while failing the off-nominal parts in the as-built state. The VIPR algorithm identified a combination of three diagnostic resonance modes that most effectively detected the defective material state in the training components. For this sample population as a whole, these resonance modes had average frequency values of approximately 81.9 kHz, 90.8 kHz, and 218.7 kHz, respectively. The PCRT inspection based on these resonance modes passed nominal dog-bone specimens and rejected off-nominal dog-bone specimens with 100% accuracy. The testing time, including data collection and analysis, was less than 5 s per part. The results are shown graphically in [figure 18](#) and in table form in [table 3](#). This sorting module required only MTS scores (scoring part similarity to the “good” population), shown on the  $y$ -axis. The  $x$ -axis is an arbitrary part index used to separate

**FIG. 17** Population characterization analysis for CalRAM Ti-6Al-4V dog-bone specimens; nominal and off-nominal as-built Ti-6Al-4V dog-bone specimens before HIP showing distinct pattern variation differences.

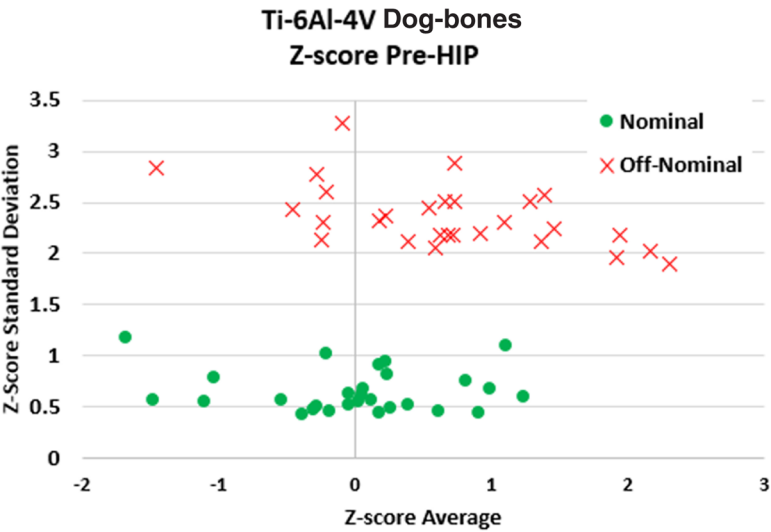
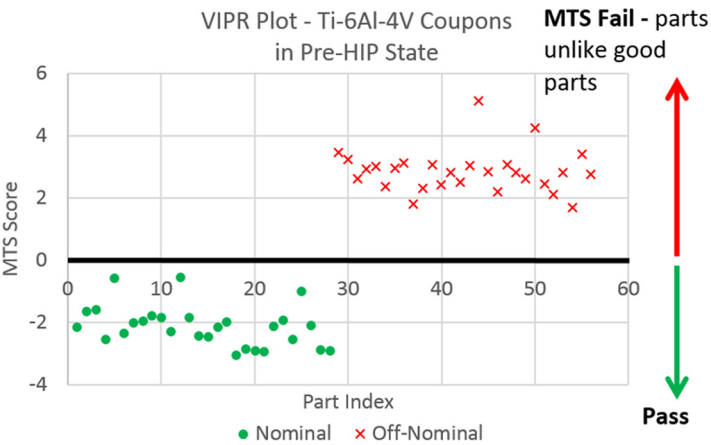


**FIG. 18** VIPR plot showing the MTS solution for sorting nominal versus off-nominal as-built Ti-6Al-4V dog-bone specimens before HIP.<sup>12</sup>



parts visually for ease of interpretation. The inspection results demonstrated PCRT detection of defective material states in additively manufactured Ti-6Al-4V material in the as-built state.

**TABLE 3** Targeted defect detection results for nominal versus off-nominal as-built Ti-6Al4V dog-bone specimens before HIP

Lot Number	Classification	State	Pass	Fail
MOR3050	Nominal	As-built	28 / 28	0 / 28
MOR3014	Off-Nominal	As-built	0 / 28	28 / 28

**PTI Analysis of HIP Effects and Post-HIP PCRT Inspection**

After the first round of testing, the samples were returned to CalRAM for HIP and then sent to Vibrant for further data collection and analysis. The samples in the post-HIP state exhibited an increase in resonance frequencies in both the nominal and off-nominal groups ([fig. 19](#)). This indicated an increase in stiffness because of HIP, which was consistent with the general expectation that HIP reduces porosity in AM components.

A PTI analysis was employed to examine the effect of HIP on the parts and determine whether the off-nominal specimens reacted in a measurably different manner from the nominal specimens. A larger frequency change in the off-nominal population would indicate a possible reduction in porosity from HIP. In general, there was significant overlap in the frequency changes ( $\Delta f$ ) for the two groups, but the average  $\Delta f$  of the off-nominal group was slightly higher than the nominal group. This indicated the possibility of a partial healing effect. The four resonance modes with the greatest difference in  $\Delta f$  between the nominal and off-nominal groups are shown in [figures 20](#) and [21](#).

**FIG. 19** Resonance spectra changes in response to HIP for individual Ti-6Al-4V specimens.

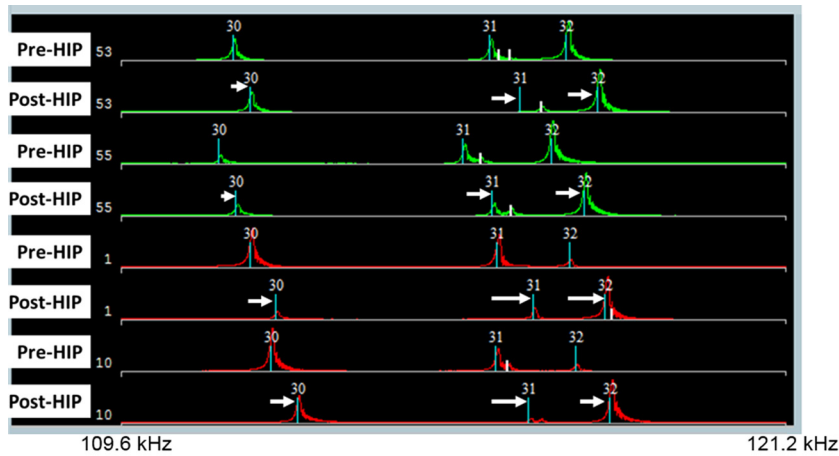


**FIG. 20** Example PTI frequency changes for different resonance modes of nominal and off-nominal Ti-6Al-4V populations.

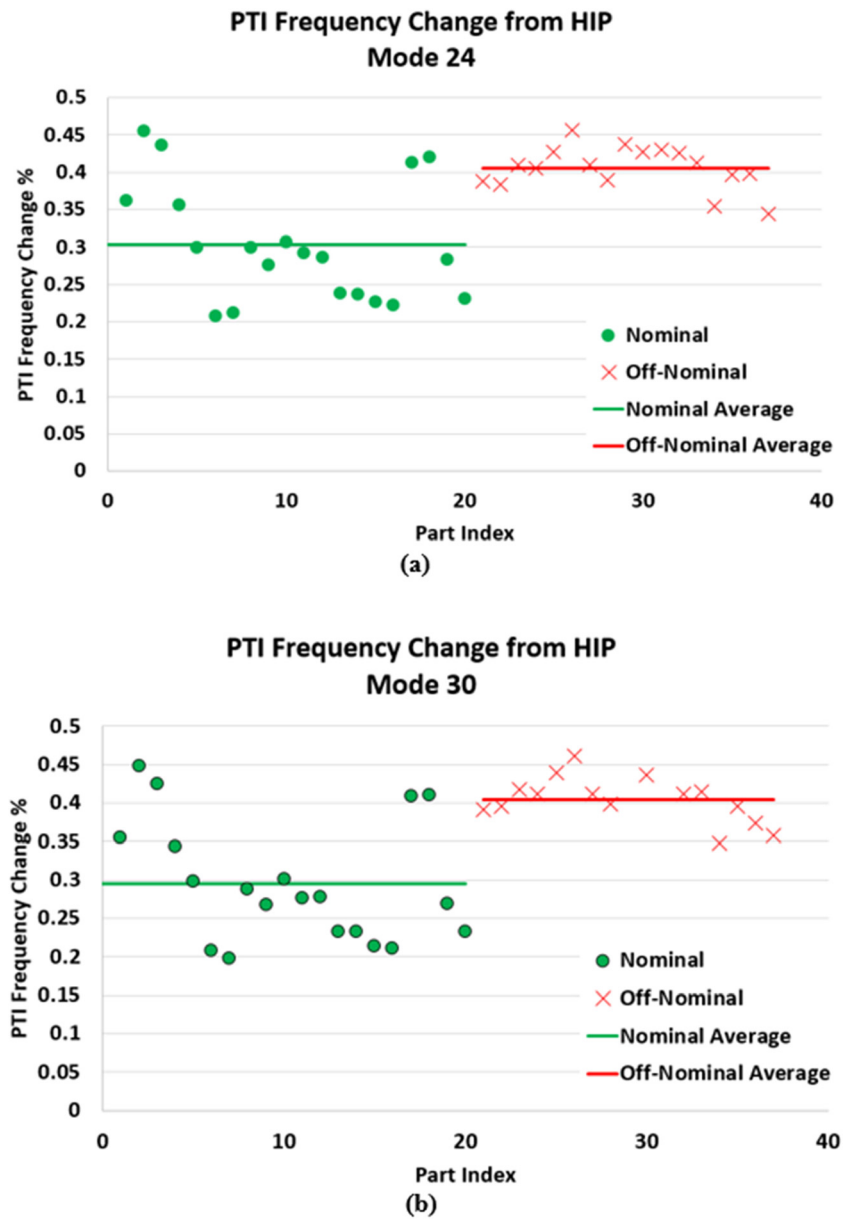


**FIG. 21** Example PTI frequency changes for different resonance modes of nominal and off-nominal Ti-6Al-4V populations.

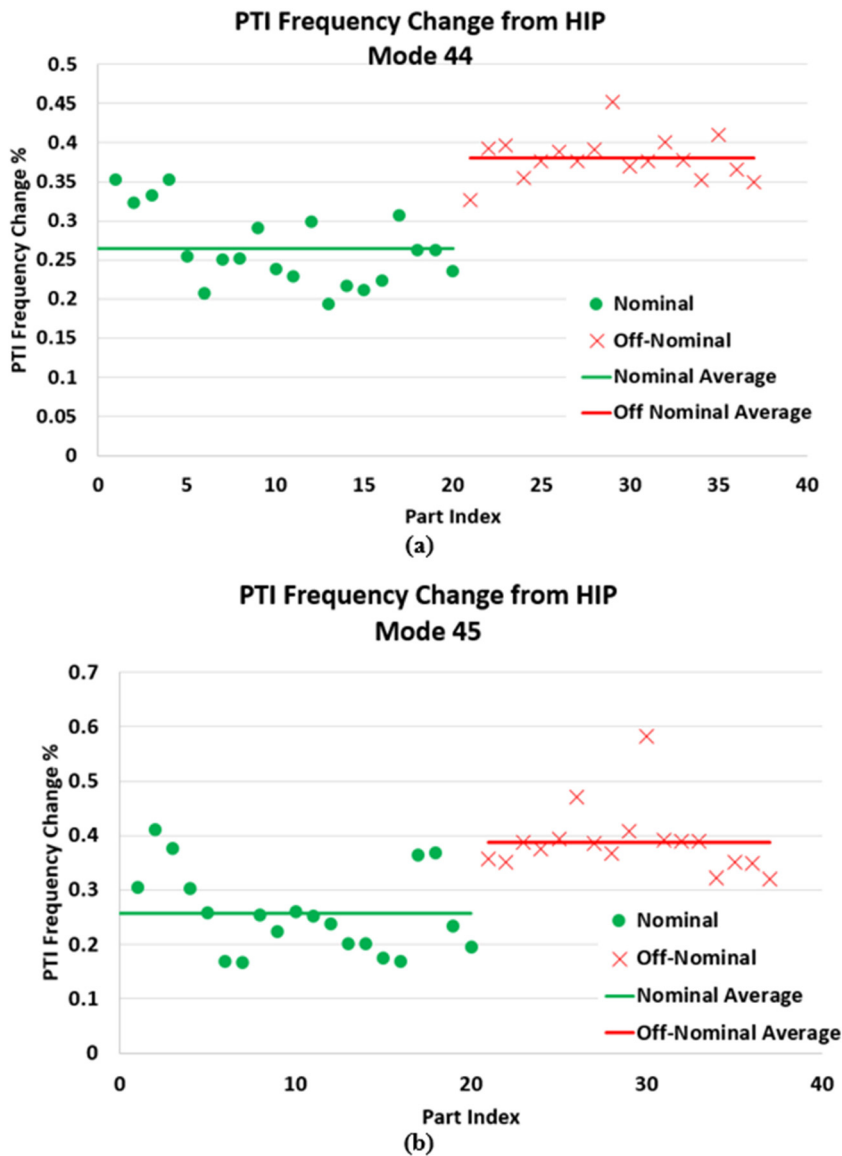
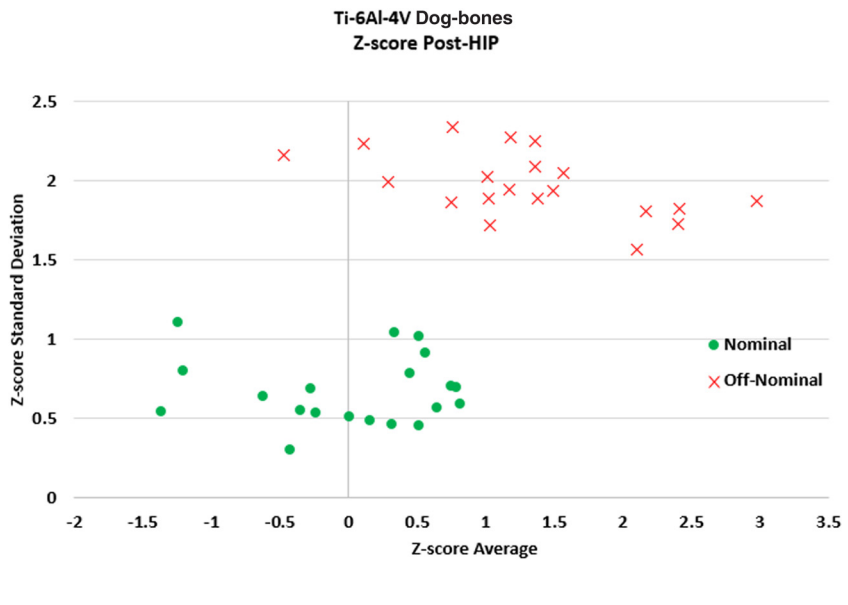


Figure 22 shows the results of a population characterization Z-score analysis of the parts in the post-HIP state. Again, 51 resonance modes were used in the Z-score calculations. The nominal parts were used as the reference set. If the HIP process

**FIG. 22** Population characterization analysis of Ti-6Al-4V dog-bone specimens in pre-HIP and post-HIP states (nominal pre-HIP parts as reference set).

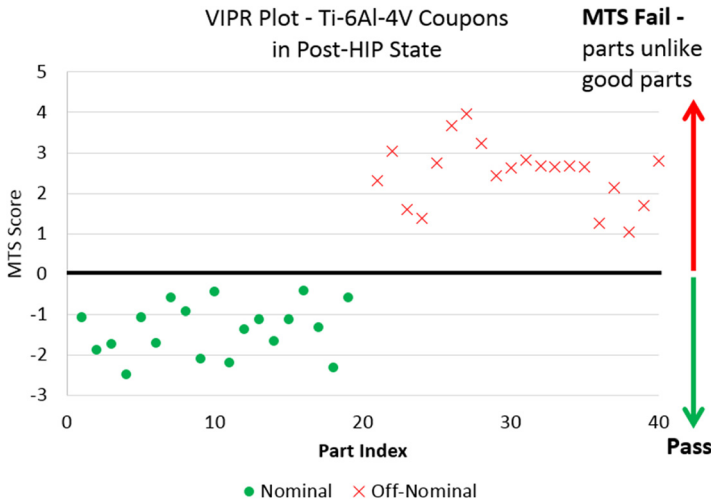


were expected to heal the off-nominal condition, the off-nominal parts would be expected to converge with the nominal population in contrast to the separation observed in [figure 17](#). The greater change in frequency in the off-nominal dog-bone specimens caused by HIP was evident in the Z-score average. The HIP process caused both the nominal and off-nominal populations to increase in frequency, and the Z-score standard deviation values (quantifying spectra pattern variation) partially converged, with a gap of about 0.5 standard deviations between the boundaries of the populations, versus a gap of about 0.9 in the pre-HIP state ([fig. 17](#)). The persisting differences in resonance behavior indicated that the HIP process did not completely heal the defective material state.

To determine whether signs of defects persisted in the post-HIP state and whether the two groups were distinguishable, another targeted defect detection sorting module was trained with a VIPR analysis to pass all specimens with nominal build parameters while failing all specimens with off-nominal material states. This analysis yielded a robust two-mode solution. For the population as a whole, these diagnostic modes had average frequency values of 160 kHz and 162 kHz, respectively. This PCRT sorting module passed the nominal specimens and failed the off-nominal specimens with 100% accuracy. The testing time, including data collection and analysis, was less than 5 s per part. The results are shown in [figure 23](#) and [table 4](#).

Even though the nominal and off-nominal populations increased in similarity after HIP, they were still easily distinguishable. The results demonstrated that

**FIG. 23** VIPR plot showing the MTS solution for sorting nominal and off-nominal Ti-6Al-4V dog-bone specimens in the post-HIP state.



PCRT could detect defective materials states in either the as-built or post-HIP states. These results led to questions about the healing effects of HIP. HIP may have incompletely healed porosity in the microstructure. It is also possible that even if HIP closed pores, other material state differences remained and were still detectable by PCRT. Finally, the as-built off-nominal components may have had little or no porosity but had other material state differences from the nominal components, such as elongated grains, that may have been more affected, but not corrected, by HIP.

The CalRAM dog-bone study demonstrated PCRT capabilities for detection of off-nominal material states produced by AM-built process variation. The study also demonstrated PCRT sensitivity to the effects of HIP on metal components. PCRT targeted defect detection is sensitive to off-nominal conditions, and a PTI analysis could be used as a process monitoring and control tool to quantify the effects of HIP.

**TABLE 4** Targeted defect detection results for nominal versus off-nominal as-built Ti-6Al-4V dog-bone specimens after HIP

Lot Number	Classification	State	Pass	Fail
MOR3050	Nominal	Post-HIP	20 / 20	0 / 20
MOR3014	Off-Nominal	Post-HIP	0 / 20	20 / 20

**Mechanical Testing and Additional Characterization of Post-HIP Dog-bone Specimens**

Follow-up characterization and mechanical testing was performed on the Ti-6Al-4V dog-bone specimens to verify component material states and generate performance data for correlation to PCRT results. Northrop Grumman performed CT, tensile testing, and fractography on a subset of nominal and off-nominal samples. Two batches of samples were evaluated. Samples were selected based on their position in the post-HIP Z-score plot. [Figure 24](#) shows the post-HIP Z-score plot with samples labeled. Both the nominal and off-nominal samples were chosen to cover a range of positions on the Z-score plot. [Table 5](#) enumerates the specimens chosen and their respective Z-score positions (described relative to each specimen’s own population).

CT scans were performed on nominal specimens 55, 41, and 47, and on off-nominal specimens 2, 10, 21, and 26. A 1.5-cm-long (0.6-in.-long) area of the gauge section was scanned ([fig. 25](#)). The CT scans found no detectable pores in any samples. Other researchers have measured volumetric porosity content in AM samples.<sup>13,14</sup> Nominal CT capability for porosity quantification has been reported<sup>13</sup> for a micro-CT system as having a gun voltage of 230 kV, current of 100  $\mu$ A, timing per frame of 1,000 ms, 0.5-mm-thick Cu filter, and voxel size of about 18  $\mu$ m. The overall porosity present is then determined using commercially available software,

**FIG. 24** Post-HIP Z-score population characterization of CalRAM Ti-6Al-4V dog-bone specimens with specimens labeled.

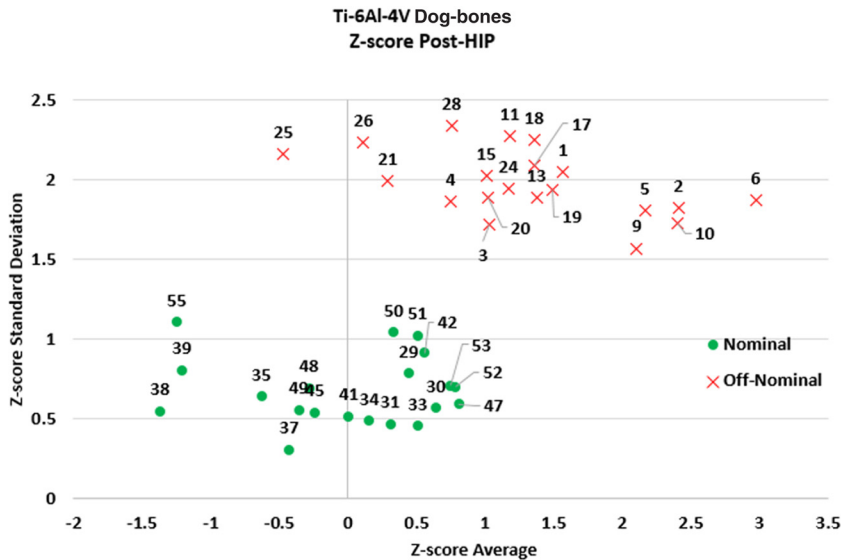
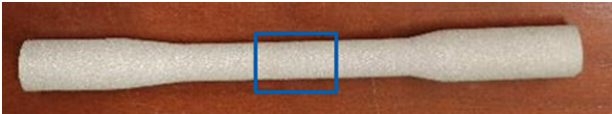


**TABLE 5** Post-HIP Ti-6Al-4V specimens sent to Northrop Grumman

Sample Batch	Specimen Number	Material State	Z-score Average	Z-score Standard Deviation
1	55	Nominal	Low	High
1	47	Nominal	High	Low
1	41	Nominal	Medium	Low
1	25	Off-Nominal	Low	High
1	6	Off-Nominal	High	Low
1	24	Off-Nominal	Medium	Medium
2	2	Off-Nominal	High	Low
2	10	Off-Nominal	High	Low
2	21	Off-Nominal	Low	Medium
2	26	Off-Nominal	Low	High

**FIG. 25** Ti-6Al-4V dog-bone specimen with CT scanning area indicated (approved for public release: NG 18-1423 July 2, 2018).



which allows for the compression of different CT slices of a given volume into a single image. The result is an overlapped image of all the slices, portraying all the defects present in the volume analyzed. [Figure 26](#) shows a Northrop Grumman CT scan of off-nominal specimen 26, which was typical for the population. Some scans, such as one for nominal specimen 55 ([fig. 27](#)), indicated faint LOF signatures on a scale of approximately  $2.5 \times 1.25$  mm (ca.  $0.10 \times 0.050$  in.), but these results were considered insignificant.

All of the selected specimens were then tensile tested to failure. Fractography analysis of the break faces was conducted. All nominal samples and some off-nominal samples showed no indication of significant pores on the fracture surface. [Figure 28](#) shows a typical result for the nominal samples (specimen 55). Some off-nominal dog-bone specimens showed possible indications of LOF in the gauge section, but these were limited to small individual pores and not volumetric porosity. [Figure 29](#) shows the result for off-nominal specimen 24.

Comparison of the stress-strain data of post-HIP specimens ([figs. 30](#) and [31](#)) showed small but measurable differences between the nominal and off-nominal populations, paralleling the differences evident in the PCRT results ([figs. 23](#) and [24](#)). A numerical summary of the tensile test data plotted in [figure 30](#) is given in [table 6](#). On average, the yield strength (offset 0.2%) of off-nominal specimens was

**FIG. 26** CT scan images for Ti-6Al-4V specimen 26 with no detectable pores observed (approved for public release: NG 18-1423 July 2, 2018).

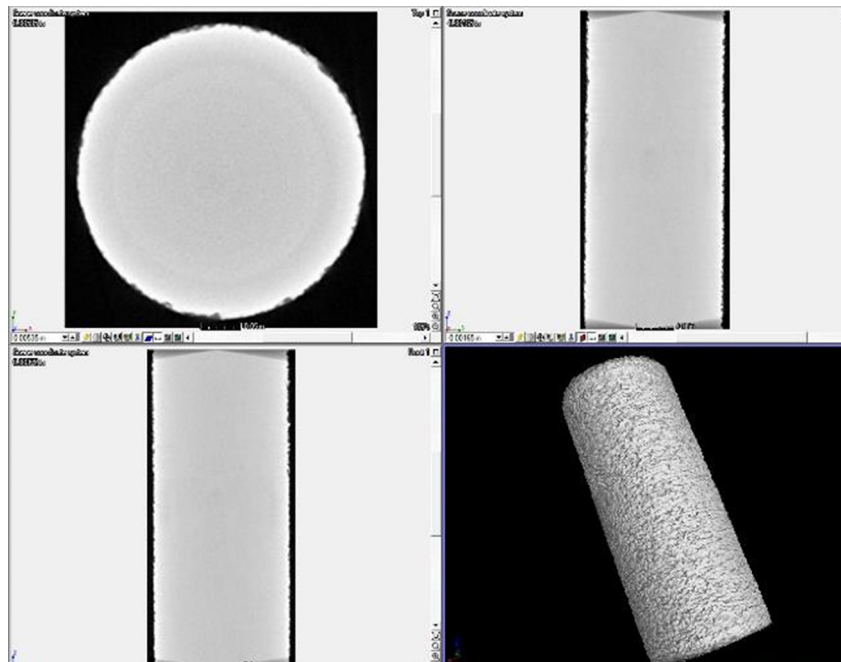


**FIG. 27** CT scan of nominal Ti-6Al-4V specimen 55 with faint LOF signatures (typical) (approved for public release: NG 18-1423 dated July 2, 2018).

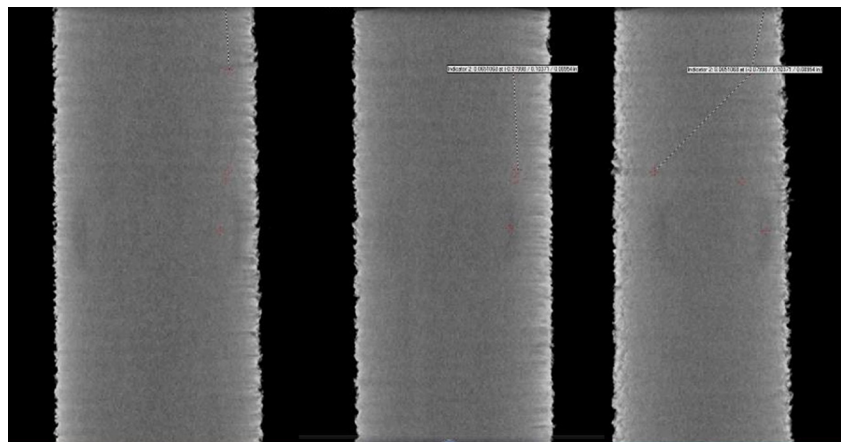


**FIG. 28** Fractography results for nominal Ti-6Al-4V specimen 55 with no indication of large pores on the fracture surface (approved for public release: NG 18-1423 dated July 2, 2018).

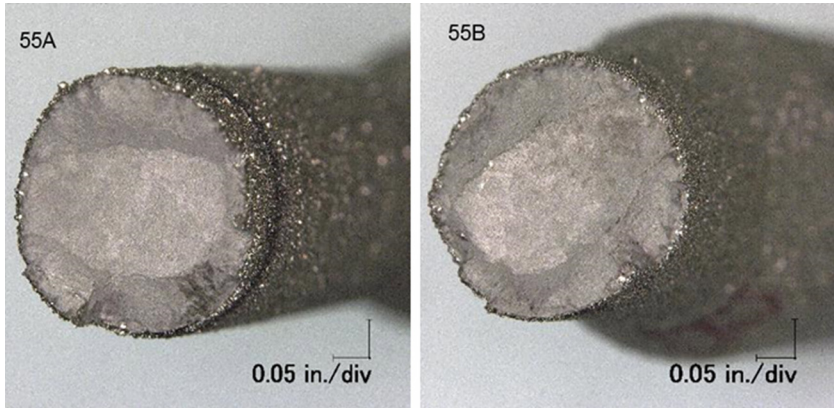
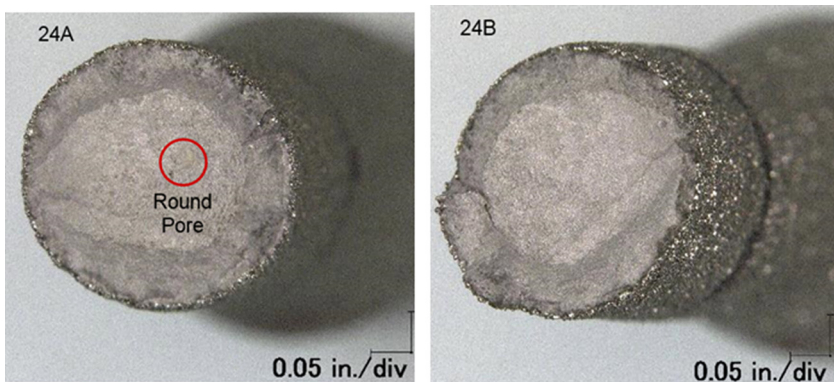


**FIG. 29** Fractography results for off-nominal Ti-6Al-4V specimen 24 with possible indication of LOF in the gauge section (approved for public release: NG 18-1423 dated July 2, 2018).



3.8% lower than that of the nominal specimens, whereas the ultimate tensile strength for the off-nominal specimens was 2.5% lower than the nominal specimens. The ultimate elongation for the off-nominal specimens was 1.12% higher than the nominal specimens. [Figure 31](#) also shows that all of the off-nominal samples failed at lower stress values than the nominal specimens, with the failure stress values for off-nominal specimens 6, 10, and 26 being significantly lower. Additionally,

**FIG. 30** Stress-strain data for nominal and off-nominal populations of post-HIP Ti-6Al-4V dog-bone specimens (approved for public release: NG 18-1423 dated July 2, 2018).

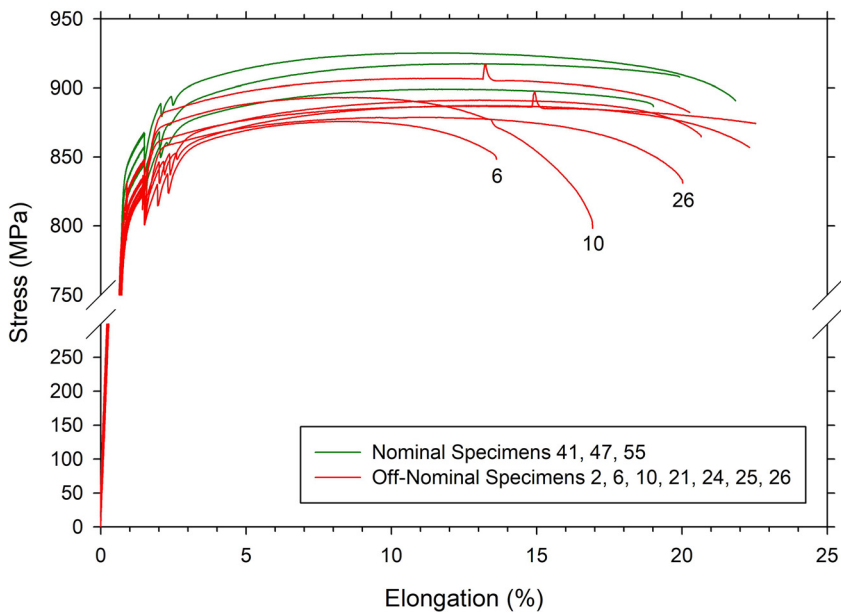


**TABLE 6** Tensile testing results for post-HIP Ti-6Al-4V specimens

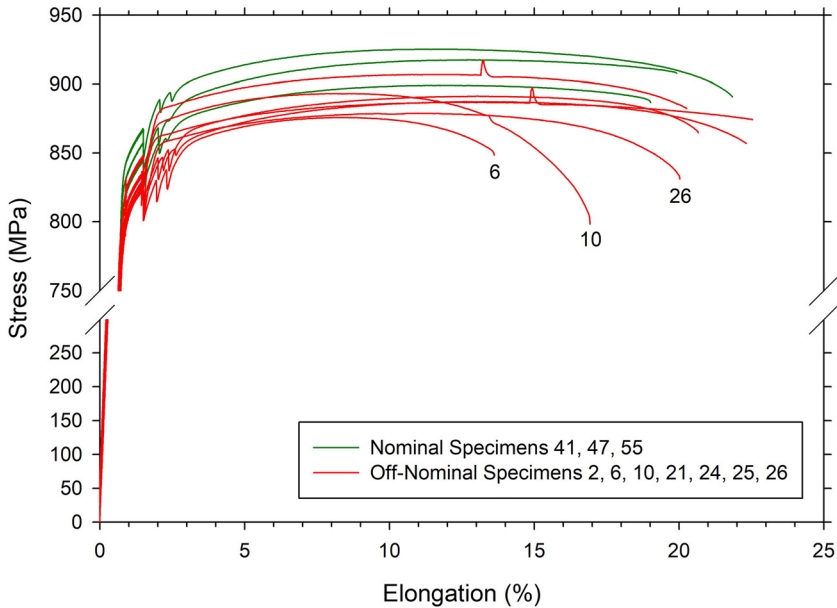
	Average Yield Strength (Offset 0.2%) MPa (ksi)	Yield Strength Standard Deviation	Average Ultimate Strength MPa (ksi)	Ultimate Strength Standard Deviation	Ultimate elongation (%)	Ultimate Elongation Standard Deviation
Nominal	834 (121)	13.8	914 (133)	11.0	20.3%	1.2
Off-nominal	802 (116)	9.6	892 (129)	12.7	20.5%	3.9
Difference of off-nominal from nominal	−3.8%		−2.5%		+1.1%	

*Note:* Approved for public release: NG 18-1423 dated July 2, 2018.

off-nominal specimens 6 and 10 appear to have failed prematurely relative to the rest of the population.

Possible correlations between the PCRT and mechanical test data were examined. For example, the occurrence of increasing *Z*-score average appeared to be weakly correlated with the yield strength values for the nominal Ti-6Al-4V

**FIG. 31** Stress-strain data for nominal and off-nominal for post-HIP Ti-6Al-4V dog-bone specimens. Detail view between 750 and 950 MPa (approved for public release: NG 18-1423 dated July 2, 2018).

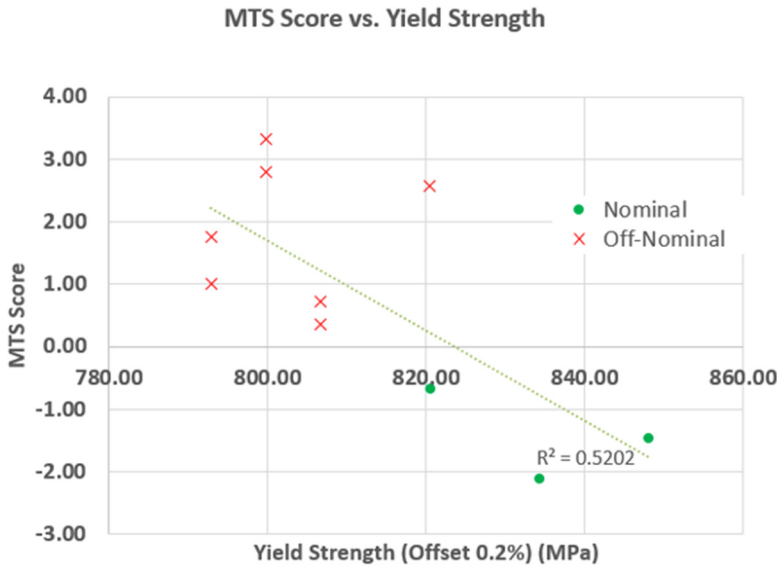


population (fig. 32 and table 7). Correlations between mechanical performance and Z-score results for the off-nominal Ti-6Al-4V population were less compelling or clear. This can be attributed to the localized nature of the defective material states built into the dog-bone specimens by CalRAM. Limiting the defective areas to the gauge section and one grip would be expected to affect some modes more than others, rather than to produce a bulk difference in frequency that would drive a Z-score average difference. The difference in Z-score standard deviation values and indicator of resonance spectra pattern differences met that expectation. Tensile testing of more samples and follow-up metallography would be required to determine whether there was a conclusive correlation between the MTS and Z-score and mechanical test results for this population.

Trends between the mechanical testing results and MTS values used in targeted defect detection sorting were also evaluated. Figure 33 shows a plot of PCRT MTS score (used for pass/fail NDT for targeted defect conditions) versus yield strength. A general trend of decreasing MTS score (indicating increasing similarity with the central tendency of the nominal population) with increasing yield strength was observed. This trend lacked sufficient data points to be considered a robust correlation, but it could be evaluated further with tensile testing of additional samples.



**FIG. 33** MTS score versus tensile yield strength (offset 0.2%) for post-HIP Ti-6Al-4V specimens.



region of the dog-bone specimens. These observations suggest the material state differences measured by PCRT were caused by something other than porosity or LOF-type flaws. Elongated grains in the off-nominal population have been hypothesized as a material state difference that could produce the difference in mechanical performance without being visible to fractography or CT but would still affect the resonance frequencies of the specimen. Metallographic examination of the samples would be the next logical step to evaluating this hypothesis.

Comparing the processing methods used in this study to produce off-nominal EB-PBF Ti-6Al-4V samples, with the processing methods used in Brown, Jones, and Tilson<sup>15</sup> to produce H-LOF flaws in LB-PBF Inconel 719 samples is instructive. In the former case, the larger 70- $\mu\text{m}$ -layer thickness used to make off-nominal Ti-6Al-4V samples resulted in a lower effective energy density than was used for nominal samples made with the uniform 50- $\mu\text{m}$ -layer thickness. The lower energy density, in turn, was expected to produce LOF porosity or unmelted powder. In the latter case, H-LOF flaws have been reported to be generated by low-power/high-speed settings, attenuated laser, or spatter falling on surface.<sup>15</sup> In both cases, regardless of the different process inputs, small decreases in the ultimate tensile strength, and even larger decreases in the percent elongation were noted.

This study was limited to follow-up characterization and mechanical testing of the specimens in the post-HIP state. The PCRT results for the specimens in the

as-built state (figs. 17 and 18) demonstrated sensitivity to the material state differences that existed before HIP. Mechanical testing of a population of pre-HIP specimens would determine the effects of nominal and off-nominal pre-HIP material states on performance. These results could be compared with the post-HIP data generated in this study to produce an evaluation of the effect of HIP on both material states. Follow-up characterization with CT and fractography would determine whether the material state differences detected by PCRT were variations in LOF porosity or indicated another property related to the layer thickness variation used in the build of these specimens.

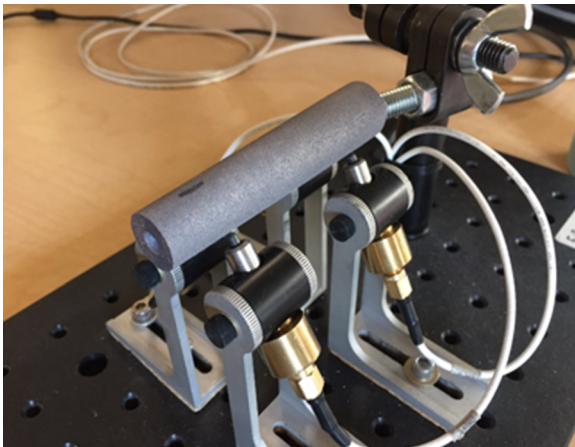
A more comprehensive PCRT evaluation would include multiple builds of nominal and off-nominal specimens, ideally some from the same machine and others from other machines. Sensitivity to material states of interest must be evaluated in the midst of normal, acceptable process variation. Although specimen-to-specimen variation within single builds was included in this study, operational PCRT inspections should factor in build-to-build and machine-to-machine variation as well. In operational PCRT inspections in manufacturing and sustainment environments, PCRT has demonstrated high levels of sensitivity to off-nominal material states in components made with AM.

#### PCRT ANALYSIS OF ALSi10MG LB-PBF SPECIMENS

##### Data Collection and Identification of Build Position Trends

A V-block fixture was configured for the AlSi10Mg cylindrical specimens from Incodema3D (fig. 34). All samples were swept from 5 to 270 kHz. Across that frequency range, 43 resonance modes were included in the analysis.

**FIG. 34** PCRT fixture showing a mounted Incodema3D AlSi10Mg specimen.



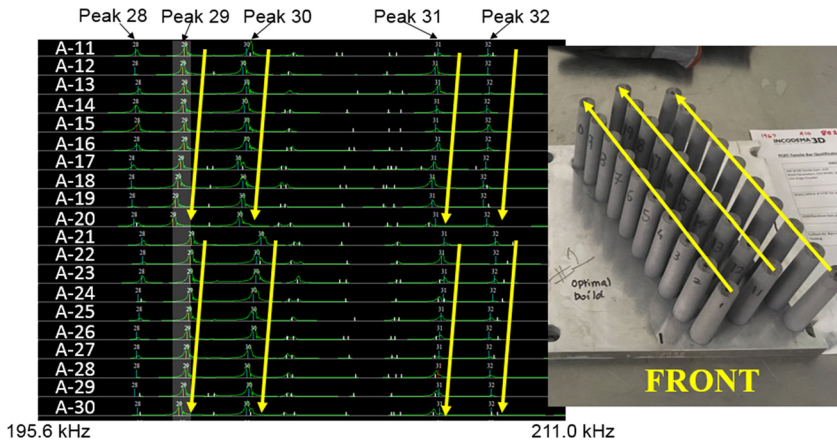
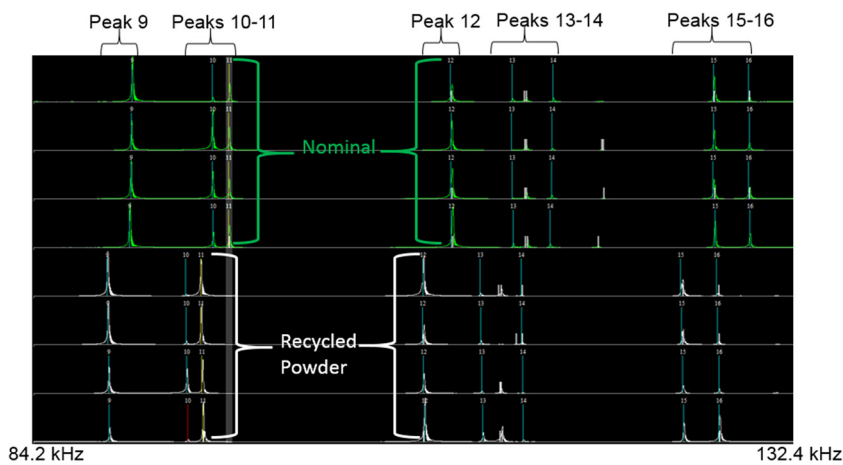
**FIG. 35** Resonance frequency trends versus build position for AlSi10Mg specimens.

Figure 35 shows stacked resonance spectra for the Serial A population (virgin powder, nominal build parameters, nominal heat treatment). Once the samples were organized in ascending numerical order according to their original position on the build plate, a frequency trend was observed. The resonance frequencies for multiple modes showed a trend of decreasing frequency from the front of the build plate to the back. This indicated a difference in elastic properties related to the build plate position. Incodema3D attributed this trend to the location of vents in the build chamber (on the front and right side of the build plate in the view shown in fig. 35). Asymmetrical ventilation could be expected to cause localized differences in atmospheric chemistry, melt-pool cooling rates, and laser-scattering or attenuating airborne particulates. All of these variations would affect the material properties of individual specimens in the build.

### Analysis of Feedstock Powder Variation

A comparison of feedstock powder was made by visually and quantitatively comparing frequencies for the components made with virgin powder (Serial A and B) to those for the components made with recycled powder (Serial C). Figure 36 highlights the differences by showing four Serial A parts stacked above four Serial C parts. Serial C parts showed distinctly lower frequencies throughout the spectra, indicating measurably lower elastic properties for the recycled powder materials. This was consistent with Incodema3D's historical data, which has found that components made with recycled powder tend to exhibit lower values for Young's modulus than those made with virgin powder. One hypothesis for this difference offered by Incodema3D was that compositional variation between virgin and recycled powder could change the stacking fault energy, altering dislocation generation and

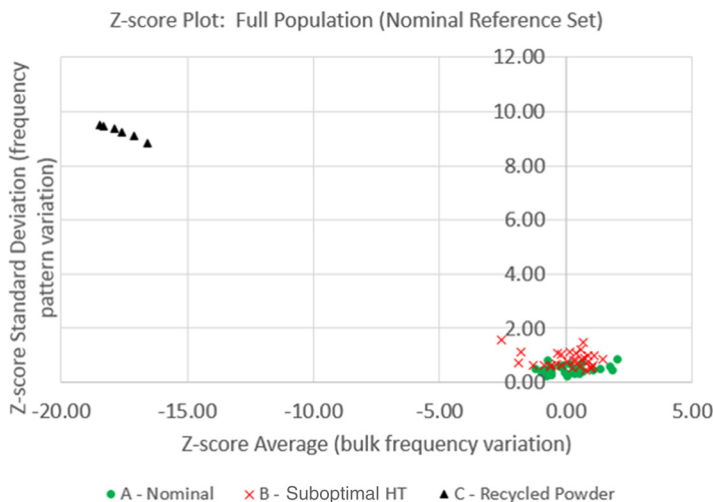
**FIG. 36** Resonance spectra comparison of nominal (virgin powder) and recycled powder AlSi10Mg specimens.



mobility. That would affect the onset of plasticity and likely the Young’s modulus. Plasticity onset and Young’s modulus also could be affected by the presence of oxides and other impurities that could be found in recycled powder.

A quantitative analysis of virgin versus recycled powder was performed with PCRT population characterization Z-score analysis (fig. 37) using all 43 resonance

**FIG. 37** Population characterization analysis showing all AlSi10Mg sample groups.<sup>12</sup>



modes in the database. The Serial A population was used as the reference set. The Serial A and Serial B populations overlapped significantly, but the Serial C specimens were extreme outliers in both Z-score average and standard deviation (more than 15 standard deviations in Z-score average), indicating both bulk and pattern frequency differences. This demonstrated that differences in feedstock powder affect resonance frequencies. A PCRT outlier screening inspection, with a boundary drawn around the virgin powder population, would easily detect components made from recycled powder.

### Analysis of Heat Treatment Variation

The other variation within the three build lots was the heat-treatment process. Because Serial A and Serial B both used optimal build parameters and virgin powder, the differences between their resonance spectra were subtle. Some resonance modes, however, were observed to have visually different behavior. Figure 38 shows an example of a mode (peak 40) that fell outside of the range of nominal variation (vertical gray band) for some Serial B parts, indicating that some modes were sensitive to the suboptimal heat treatment.

Excluding the recycled powder from the population characterization plot in figure 37 allowed a more detailed view of the Serial A versus Serial B comparison. As shown in figure 39, although the overlap between the two lots was significant, Serial B as a group had wider ranges of variation in both Z-score average and standard deviation. This larger range of variation in the Serial B specimens was consistent with the nonuniform cooling rates that were part of the suboptimal heat-

**FIG. 38** Resonance spectra comparison of nominal with suboptimal heat-treatment AISi10Mg specimens.

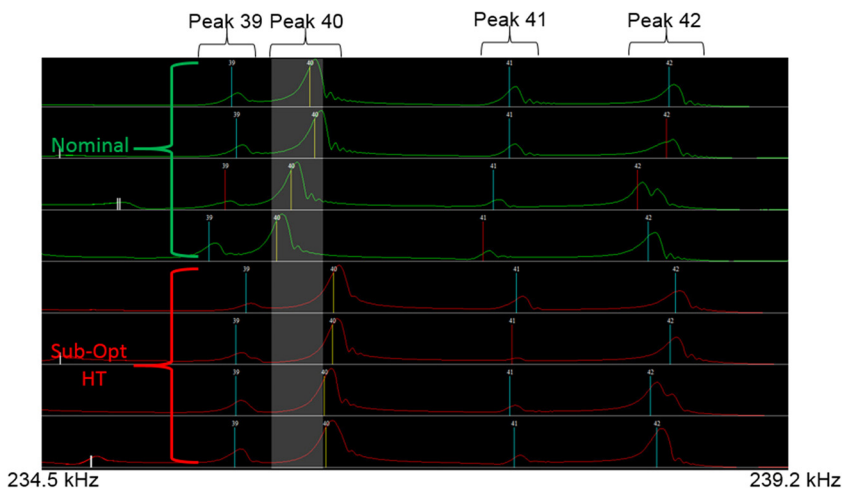
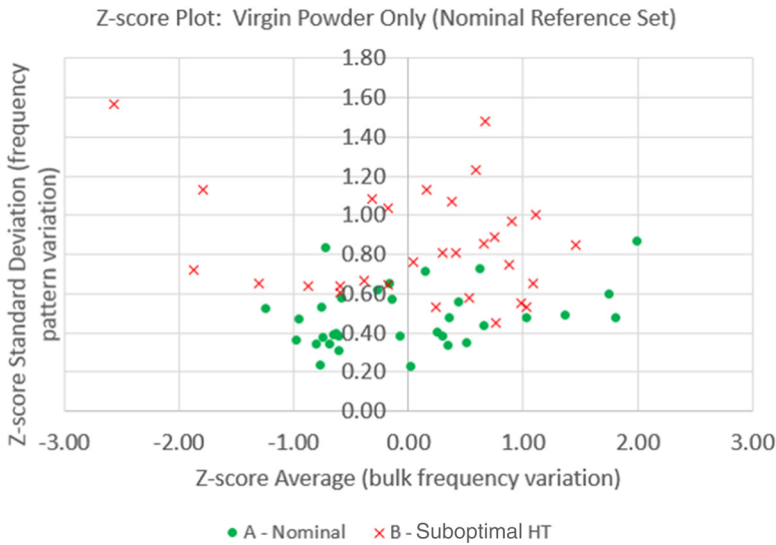


**FIG. 39** Population characterization analysis detail view of nominal versus suboptimal heat treatment of AlSi10Mg specimens.



treatment process for that population. The large amount of overlap in the Serial A and B populations meant that a targeted defect detection inspection would be required for effective inspection of variations caused by heat treatments.

A targeted defect detection sort was configured to detect the suboptimal heat-treatment condition. The Serial A (nominal) parts were trained as the acceptable population and the Serial B (suboptimal heat treatment) parts were trained as the unacceptable population. The recycled powder components were left out of the training set. The VIPR algorithm configured a sorting module that used a set of three diagnostic modes. For the population as a whole, the average frequency values for these three modes were 90.3 kHz, 200.1 kHz, and 236.0 kHz. The sorting module required only the MTS score (scoring similarity to the good population) for part sorting. The testing time, including data collection and analysis, was less than 5 s per part. The VIPR sort passed the nominal components and failed the off-nominal components with 100% accuracy. [Figure 40](#) shows the VIPR plot for the sorting module. The *y*-axis is the MTS score, and the *x*-axis is an arbitrary part index used to separate parts horizontally for ease of interpretation. [Table 8](#) summarizes the results.

The Incodema3D cylinder study demonstrated PCRT capabilities for detection of heat-treatment process variation and base material differences in metallic powder. Additional characterization of this population would be helpful to generate data for correlation to resonance frequencies. Destructive characterization of the microstructure for a subset of these samples could provide more insight into the

**FIG. 40** VIPR plot showing the MTS solution for sorting nominal and suboptimal heat treatment of AlSi10Mg specimens.

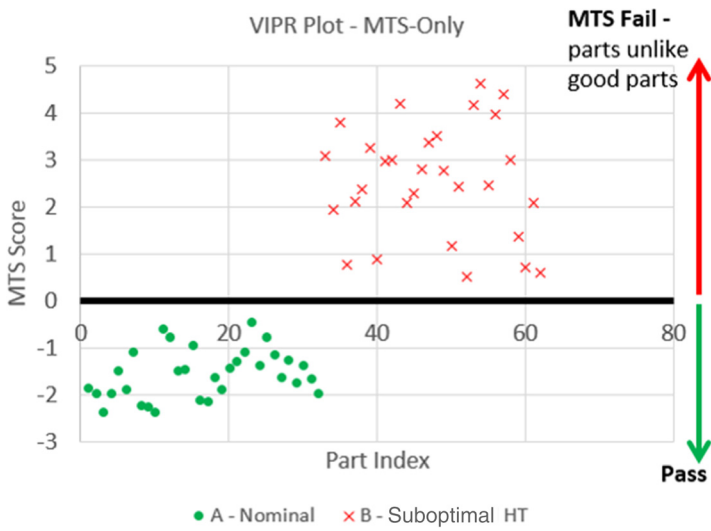


**TABLE 8** Targeted defect detection results for sorting nominal and suboptimal heat treatment of AlSi10Mg specimens

Lot	Classification	Heat Treatment	Pass	Fail
Serial A	Nominal	Optimal	30 / 30	0 / 30
Serial B	Off-Nominal	Suboptimal	0 / 30	30 / 30

material state variations that were detected in the suboptimal heat-treatment and recycled powder specimens. A more in-depth study of the build position trends observed in this population could be informative.

Capturing additional normal process variation is recommended. Each condition was represented by only one build of specimens. Logging of multiple builds of nominal components would be required to quantify normal process variation before a production PCRT sort could be implemented.

## Conclusions

This study demonstrated PCRT detection of differences in the material state of additively manufactured parts caused by feedstock, processing, and post-processing variation. Detection of defective material states caused by process variation was demonstrated with EB-PBF Ti-6Al-4V dog-bone populations provided by CalRAM in both the pre-HIP and post-HIP states. Follow-up mechanical testing at Northrop

Grumman of post-HIP specimens confirmed a performance difference between the nominal and off-nominal populations, with small differences in yield strength, ultimate tensile strength, and elongation at failure observed. PCRT detection of nominal versus off-nominal material state differences paralleled the differences exhibited by mechanical properties of post-HIP specimens. A second round of mechanical testing on nominal and off-nominal specimens in the pre-HIP state is recommended to generate mechanical performance data for correlation to the pre-HIP PCRT results. Operationally, there are numerous advantages to PCRT screening of as-built parts before performing HIP or other expensive, time-consuming post-processing steps. A second recommendation is for metallographic analysis of the post-HIP Ti-6Al-4V population to determine whether an elongated grain structure in the off-nominal specimens was the reason for the resonance frequency differences detected by PCRT and the differences in mechanical performance.

PCRT detection of feedstock powder variation and post-process heat-treatment variation was demonstrated with the AlSi10Mg specimens provided by Incodema3D. In addition, quantification of differences between specimens made with recycled and virgin powder with PCRT and detection of suboptimal heat treatment using PCRT inspection were demonstrated.

These studies were limited in scope because batch-to-batch and machine-to-machine variations were not included in the sample populations. An analysis of process variation between multiple builds and machines would be required to comprehensively quantify variation in nominal populations and sensitivity to off-nominal material states in the midst of that variation. This is a regular aspect of implementing an operational PCRT inspection for AM.

## ACKNOWLEDGMENTS

The authors wish to thank the ASTM E07.10 WK47031 community for creating an engaged and collaborative group of professionals dedicated to improving the state-of-the-art for NDT of parts made additive manufacturing, thereby improving their safety and reliability. The authors also wish to thank the MB CalRAM, LLC., Northrop Grumman Aerospace Systems, Incodema3D, NASA White Sands Test Facility, and Aerojet-Rocketdyne organizations for making their representatives and resources available for this study.

## References

1. *Standard Guide for Nondestructive Examination of Metal Additively Manufactured Aerospace Parts after Build*, ASTM E3166-20 (West Conshohocken, PA: ASTM International, approved February 1, 2020), <http://doi.org/10.1520/E3166-20>
2. S. James, J. M. Waller, M.-C. Ebert, H. Gong, R. Grylls, J. Middendorf, E. Biedermann, K. LaCivita, J. Brausch, T. Nakagawa, C. Peitsch, B. Trethewey, M. White, E. Ginzel, C. Kretzer, T. Mayer, and S. Singh, "Representative NDE Round Robin Results on Metal Additively Manufactured Test Parts and Physical Reference Standards," *ASTM Materials Performance and Characterization* (in review).

3. E. Todorov, R. Spencer, S. Gleeson, M. Jamshidinia, and S. M. Kelly, *America Makes: National Additive Manufacturing Innovation Institute (NAMI) Project 1: Nondestructive Evaluation (NDE) of Complex Metallic Additive Manufactured (AM) Structures*, AFRL-RX-WP-TR-2014-0162, EWI (Cincinnati, OH: Air Force Research Laboratory, Materials and Manufacturing Directorate, Wright-Patterson Air Force Base, June 2014).
4. J. W. Waller, B. H. Parker, K. L. Hodges, E. R. Burke, J. L. Walker, and E. R. Generazio, *Nondestructive Evaluation of Additive Manufacturing State-of-the-Discipline Report*, NASA/TM-2014-218560 (Houston, TX: NASA Johnson Space Center, November 1, 2014).
5. M. Seifi, M. Gorelik, J. Waller, N. Hrabe, N. Shamsaei, S. Daniewicz, and J. J. Lewandowski, "Progress towards Metal Additive Manufacturing Standardization to Support Qualification and Certification," *Journal of the Materials, Minerals, Metals and Materials Society* 69, no. 3 (2017): 439–455.
6. *Standard for Additively Manufactured Spaceflight Hardware by Laser Powder Bed Fusion in Metals*, MSFC-STD-3716 (Huntsville, AL: NASA Marshall Space Flight Center, October 18, 2017).
7. *Standard Test Methods for Tension Testing of Metallic Materials*, ASTM E8/E8M-16ae1 (West Conshohocken, PA: ASTM International, approved August 1, 2016), [http://doi.org/10.1520/E0008\\_E0008M-16AE01](http://doi.org/10.1520/E0008_E0008M-16AE01)
8. *Standard Guide for Resonant Ultrasound Spectroscopy for Defect Detection in Both Metallic and Non-Metallic Parts*, ASTM E2001-18 (West Conshohocken, PA: ASTM International, approved November 1, 2018), <http://doi.org/10.1520/E2001-18>
9. *Standard Practice for Process Compensated Resonance Testing via Swept Sine Input for Metallic and Non-Metallic Parts*, ASTM E2534-15 (West Conshohocken, PA: ASTM International, approved December 1, 2015), <http://doi.org/10.1520/E2534-15>
10. *Standard Practice for Outlier Screening Using Process Compensated Resonance Testing via Swept Sine Input for Metallic and Non-Metallic Parts*, ASTM E3081-16 (West Conshohocken, PA: ASTM International, approved December 1, 2016), <http://doi.org/10.1520/E3081-16>
11. *Standard Practice for Part-to-Itself Examination Using Process Compensated Resonance Testing via Swept Sine Input for Metallic and Non-Metallic Parts*, ASTM E3213-19 (West Conshohocken, PA: ASTM International, approved May 1, 2019), <http://doi.org/10.1520/E3213-19>
12. Vibrant Corporation, "PCRT Resonance Solutions—Additive Manufacturing," 2018 <http://web.archive.org/web/20190206172145/https://www.vibrantndt.com/download/736/>
13. A. D. Brandão, J. Gumpinger, M. Gschweiltl, C. Seyfert, P. Hofbauer, and T. Ghidini, "Fatigue Properties of Additively Manufactured AlSi10Mg—Surface Treatment Effect" *Procedia Structural Integrity* 7 (2016): 58–66.
14. A. du Plessis, I. Yadroitsev, I. Yadroitsava, and S. G. Le Roux, "X-Ray Microcomputed Tomography in Additive Manufacturing: A Review of the Current Technology and Applications," *3D Printing and Additive Manufacturing* 5, no. 3 (2018): 1–20.
15. A. L. Brown, Z. Jones, and W. Tilson, "Classification, Effects, and Prevention of Build Defects in Powder-bed Fusion Printed Inconel 718" (paper presentation, NASA Marshall Space Flight Center, TMS 2017, 146th Annual Meeting, San Diego, CA, March 1, 2017).